Biol Cybern (2013) 107:83–94
DOI 10.1007/s00422-012-0534-2

ORIGINAL PAPER

Biological Cybernetics

Towards a large-scale model of patient-specific epileptic spike-wave discharges

Peter Neal Taylor · Marc Goodfellow · Yujiang Wang · Gerold Baier

Received: 29 June 2012 / Accepted: 17 October 2012 / Published online: 7 November 2012

Abstract Clinical electroencephalographic (EEG) recordings of the transition into generalised epileptic seizures show a sudden onset of spike-wave dynamics from a low-amplitude irregular background. In addition, non-trivial and variable spatio-temporal dynamics are widely reported in combined EEG/fMRI studies on the scale of the whole cortex. It is unknown whether these characteristics can be accounted for in a large-scale mathematical model with fixed heterogeneous long-range connectivities. Here, we develop a modelling framework with which to investigate such EEG features. We show that a neural field model composed of a few coupled compartments can serve as a low-dimensional prototype for the transition between irregular background dynamics and spike-wave activity. This prototype then serves as a node in a large-scale network with long-range connectivities derived from human diffusion-tensor imaging data. We examine multivariate properties in 42 clinical EEG seizure recordings from 10 patients diagnosed with typical absence epilepsy and 50 simulated seizures from the large-scale model using 10 DTI connectivity sets from humans. The model can reproduce the clinical feature of stereotypy where seizures are more similar within a patient than between patients, essentially creating a patient-specific fingerprint. We propose the approach as a feasible technique for the investigation of patient-specific large-scale epileptic features in space and time.

Keywords Epilepsy · EEG · Mathematical modelling · Spatio-temporal patterns · Spike-wave · Diffusion-tensor imaging

Electronic supplementary material The online version of this article (doi:10.1007/s00422-012-0534-2) contains supplementary material, which is available to authorized users.

P. N. Taylor (✉) · Y. Wang · G. Baier
Manchester Interdisciplinary Biocentre, The University of Manchester, Manchester M1 7DN, UK
e-mail: peter.taylor@postgrad.manchester.ac.uk

M. Goodfellow
Centre for Interdisciplinary Computational and Dynamical Analysis (CICADA), School of Mathematics, The University of Manchester, Manchester M13 9PL, UK

1 Introduction

A defining feature of patients with epilepsy is the occurrence of seizures, which are accompanied on the electroencephalogram (EEG) by specific changes in spatio-temporal rhythms. In this context, the background state of the EEG channels is temporally irregular and typically desynchronised. During periods of spontaneously occurring absence seizures, the temporal waveform takes on the characteristic form of a spike-wave discharge (SWD) (Weir 1965) and is accompanied by increased global correlation (Cohn and Leader 1967; Amor et al. 2005; Garcia-Dominguez et al. 2005; Aarabi et al. 2008). This is in addition to patient-specific properties (Schindler et al. 2011) which have also been noted during fMRI measurements (Moeller et al. 2010). Although large-scale synaptic networks are implicated in these generalised seizure events (Pinault and O'Brien 2005; Meeren et al. 2002; Blumenfeld 2005) it is unclear whether dynamical models incorporating such realistic, heterogeneous connectivity will support transitions to epileptic states with more globally synchronised dynamics.

Modelling seizure dynamics with SWD using dynamical systems approaches at the macroscopic scale has received much recent attention (Breakspear et al. 2006; Marten et al. 2009; Goodfellow et al. 2010; Taylor and Baier 2011; Wang et al. 2012). These models have predominantly focussed

on the temporal aspects of SWD seizures, although it has recently been shown that small network extensions to such models can have profound implications for the dynamics (Goodfellow et al. 2010, 2012a). Although each of the frameworks employed supports a natural extension to large, or whole brain models (Sotero et al. 2007; Babajani-Feremi and Soltanian-Zadeh 2010; Bojak et al. 2010), these extensions have not been used in the context of generalised epilepsy. Clearly, an important facet of the exploration of the mechanisms and properties of absence epilepsy is the investigation of macroscopic models of extended, large-scale brain networks.

Recent advances have brought to the forefront of clinical neuroscience the relevance of large-scale brain networks, as revealed for example by diffusion-tensor imaging (DTI) which has, to some extent, been validated against experimental tract tracing studies (Parker et al. 2002a) and against standard brain atlases (Parker et al. 2002b). Emerging alongside this data are modelling frameworks with which to investigate the effect of network connectivity on large-scale dynamics (Jirsa et al. 2010; Deco et al. 2011). In incorporating long-range connectivity into large-scale brain models one can distinguish two approaches. In the first of these, long range, or so-called heterogeneous connections are superposed onto a continuum formulation of propagating activity in macroscopic neural fields (Jirsa and Kelso 2000). A second approach is to discretise the connectivity in a hierarchical approach, which then naturally supports the inclusion of adjacency matrices (Breakspear and Stam 2005; Sotero et al. 2007; Babajani-Feremi and Soltanian-Zadeh 2010).

The aim of this study is to investigate patient-specific properties of epileptic seizures. To this end, we introduce a large-scale hierarchical model of SWD seizures and suggest a method by which to analyse such patient-specific properties. The large-scale model is formulated to incorporate anatomically derived human brain connectivity from the DTI of ten human subjects. We use our analysis methods to investigate patient-specific aspects of both model output and clinical seizure data.

2 Models/methods

Population level descriptions of epileptic rhythms have been attempted at various scales. Neurophysiologically motivated population models such as those based on (Jansen and Rit 1995; Breakspear et al. 2006) were used to describe the temporal properties of epileptic seizure dynamics. A key problem when dealing with more detailed models is that the analysis and understanding of their properties becomes increasingly difficult. At a higher level of abstraction, neural field models (Amari 1977; Wilson and Cowan 1972) can be employed which still retain many key properties such as firing rate transfer functions, different timescales and interactions between excitatory and inhibitory populations. Specifically, these features have been shown to be important in the context of epilepsy modelling (Wendling et al. 2002; Breakspear et al. 2006; Goodfellow et al. 2010; Taylor and Baier 2011).

Spatial extensions to both sets of models exploring physiologically relevant connectivity for cortical rhythm generation have been explored (Sotero et al. 2007; Bojak et al. 2010; Deco et al. 2011). In order to investigate the relevance of these networks for generalised epilepsies, we propose a hierarchical large-scale model based on the simplest model which incorporates the above features and is known to produce epileptic SWD. Furthermore, as we are specifically interested in spatio-temporal patterns and SWD morphology which do not require explicit representation of complex thalamocortical interaction, our work abstracts away from this detail similar to what has been done in other works (Taylor and Baier 2011; Goodfellow et al. 2010; Wang et al. 2012).

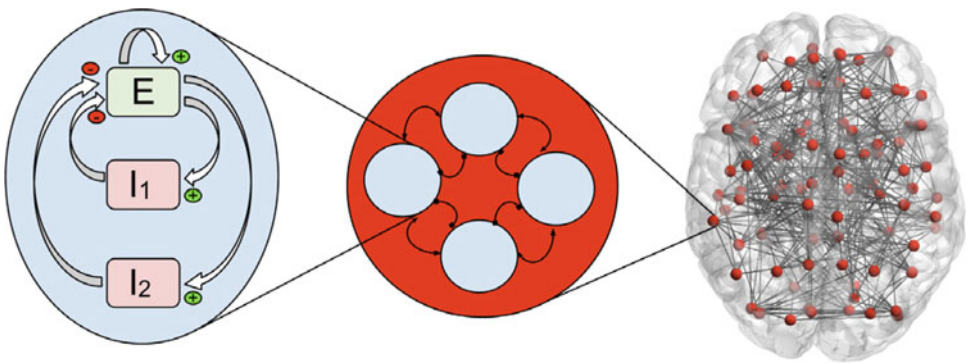

Fig. 1 A single compartment is made up of three interacting populations (E, I_1 and I_2) represented in the oval (left side of the figure). Four compartments are then coupled construct a 'node' for local dynamics. Nodes are then coupled heterogeneously using DTI data. Nodes (*red spheres*) and edges (*grey lines*) for connectivity set 1 obtained from DTI data from http://piconmat.com/ are shown on the right side of the figure. Only edges with strength greater than 0.75 are shown for illustrative purposes. All edges are included in simulations. Image generated using BrainNet viewer (http://www.nitrc.org/projects/bnv/) (Colour online)

Ultimately, we wish to build up to a whole brain scale model of epileptic activity. This is composed of heterogeneously coupled nodes, representative of activity at a local (ECoG) level, which in turn comprises coupled space-independent oscillators. An exemplary hierarchical connectivity scheme is shown in Fig. 1.

2.1 Space-independent model

As an entry point to describe local cortical dynamics, we use an extended three layer version of the two layer model described by Amari (1977). We begin with a space-independent system containing one population of excitatory neurons and two populations of inhibitory neurons that has previously been used to model SWD (Taylor and Baier 2011) and is described by the following set of ordinary differential equations (Eq. 1):

$$\begin{aligned}\dot{E}(t) &= h_1 - E + w_1\ f[E] - w_2\ f[I_1] - w_3\ f[I_2]\\ \dot{I}_1(t) &= (h_2 - I_1 + w_4\ f[E])/\tau_1\\ \dot{I}_2(t) &= (h_3 - I_2 + w_5\ f[E])/\tau_2\end{aligned} \tag{1}$$

In this model, an excitatory population (E) is self-exciting and also drives two inhibitory populations ($I_{1,2}$). The inhibitory populations operate at different time scales ($\tau_{1,2}$) and inhibit the excitatory population via negative feedback. Input from one population to another is mediated by a firing rate transfer function (f) multiplied by a connectivity parameter ($w_{1,\ldots,5}$). In place of the Heaviside step function used originally by Amari, we incorporate a piecewise linear (PWL) transfer function as an approximation to the physiologically plausible (Eeckman and Feeeman 1991) sigmoid function. The PWL function is defined as follows:

$$f(v) = \begin{cases} 0, & v \le -l \\ (v+l)/2l, & -l < v < l \\ 1, & v \ge l \end{cases}, \tag{2}$$

where $v = E, I_1$ or I_2, and $l > 0$ determines the steepness of the transition and is a parameter.

Finally, additive constants ($h_{1,2,3}$) are included as in the original Amari model. Note that for $w_3 = 0$ the system reduces to a two layer model as the subsystem E/I_1 becomes independent of I_2. Equally, for $w_5 = 0$, the equation for I_2 has a stable fixed point at solution h_3/τ_2 that is independent of the E/I_1 subsystem and, consequently, when I_2 is at fixed point, it does not affect the E/I_1 subsystem dynamically.

2.2 Multiple coupled compartments: local connectivity

Starting from Eq. 1, we construct a discrete spatial model of local dynamics using coupling between a small number of compartments with distance-dependent connectivity strengths. At the local level, these connectivities operate on three discrete levels, namely, self-coupling (w_{ks}), nearest-neighbour coupling (w_{kn}), and coupling to distant compartments (w_{kf}):

$$d_{ij}^k = \begin{cases} w_{ks}, & |i-j| = 0 \\ w_{kn}, & |i-j| = 1 \\ w_{kf}, & |i-j| > 1 \end{cases}, \tag{3}$$

where $k = E, I_1, I_2$ indexes the source of the connection, and $i, j = 1, \ldots, n$, where n is the number of local compartments. Throughout this study, we consider $w_{kf} = 0$ for simplicity, which means that local compartments are connected only to their nearest neighbours.

The equations for the local system are then as follows:

$$\begin{aligned}\dot{E}_i &= h_1 - E_i + \sum_j d_{ij}^E f[E_j] \\ &\quad - \sum_j d_{ij}^{I_1} f[I_{1j}] \\ &\quad - \sum_j d_{ij}^{I_2} f[I_{2j}] \\ \dot{I}_{1i} &= (h_2 - I_{1i} + w_4 f[E_i])/\tau_1 \\ \dot{I}_{2i} &= (h_3 - I_{2i} + w_5 f[E_i])/\tau_2\end{aligned} \tag{4}$$

which is spatially homogeneous with periodic boundary conditions.

To study the influence of this additional coupling on the dynamics of Eq.4, we investigate systems composed of a small number of compartments. Specifically, we use two, three, and four coupled compartments.

For bifurcation analysis numerical solutions were computed using the Matlab 2010a 'ode23' differential equation solver, giving time series from which the minima and maxima were recorded for a given parameter value. Forward and backward parameter scans were computed using random initial conditions, then continued using the end condition as initial conditions for the subsequent simulation with the new parameter value (to test for bistability). For Fig. 4, the type of dynamics was represented symbolically and the boundaries group the areas of qualitatively different behaviour.

2.3 Large-scale extension: long-range connectivity

Now we suggest a method by which to extend the system of a small number of coupled oscillators into larger networks of connected nodes incorporating realistic cortical coupling schemes. To this end, we use diffusion-weighted magnetic resonance imaging and probabilistic tractography connectivity information from the piconmat database.[1] This data includes connectivity obtained from ten healthy human subjects. The tractography connection maps are between

[1] http://piconmat.com.

the aparc+aseg regions defined by FreeSurfer[2] using the multi-fibre probabilistic index of connectivity (PICo) method (Parker et al. 2003) and are based on data obtained using a 3T Philips Achieva scanner. All connection matrices were inferred using 1,000 streamlines as described in Rose et al. (2009). Individual streamlines in this context are fibre tracks determined by the PICo method. Using the same number of streamlines for all subjects and not biasing the network by, for example, limiting the number of nodes or edges in the adjacency matrix, comparisons between simulated outputs can be made using non-graph theoretical measures (as detailed in Sect. 2.4).

The probabilistic connectivity is incorporated into the model in the form of a static adjacency matrix (C) with values used to indicate connection strengths between the node on the ith row and the mth column. The diagonals of this matrix are set to zero as this represents self-to-self connectivity which is already incorporated in the node as described in the previous section.

As expanded upon in the results section, each node (N) is modelled by four underlying compartments with short-range local coupling and periodic boundaries as per Eq. 4 (Sect. 2.2). In this framework, long-range (inter-node) connectivity is included as follows: each compartment of a node receives the same excitatory input from the average output of the four compartments of each connected node. Thus, the hierarchical connectivity scheme can be formalised as

$$\begin{aligned}
\dot{E}_i &= h_1 - E_i + \sum_j d^1_{ij} f[E_j] \\
&\quad - \sum_j d^2_{ij} f[I_{1j}] \\
&\quad - \sum_j d^3_{ij} f[I_{2j}] \\
&\quad + g_i \\
\dot{I}_{1i} &= (h_2 - I_{1i} + w_4 f[E_i])/\tau_1 \\
\dot{I}_{2i} &= (h_3 - I_{2i} + w_5 f[E_i])/\tau_2 \\
g_i &= \sum_{m=1}^{N_m} C_{i,m} f\left[\frac{1}{n}\sum_j E_j(t-T)\right],
\end{aligned} \tag{5}$$

where N_m is the number of nodes in the high level network specified by the adjacency matrix, C. The use of long-range excitatory coupling between nodes follows the large-scale modelling approaches of Goodfellow et al. (2012a), Deco et al. (2009), Honey and Sporns (2008), Sotero et al. (2007). Realistic time delays (T) are included into the model and are linearly scaled with Euclidian distance between nodes. Delays are grouped into seven bins with a conduction velocity of 7 m/s as in Bojak et al. (2010). Equations were solved numerically using 'dde23' in MATLAB. The parameters for all figures are summarised in Table 1.

Table 1 Model parameters

	Fig. 2	Fig. 3	Fig. 4	Fig. 5	Fig. 6
w_1, w_{Es}	0.6	0.6	0.6	0.6	0.5
w_{En}	–	0.3	varies	0.3, 0.45	0.3
$w_2, w_{I_1 s}$	1.3	1.3	1.3	1.3	1.95
$w_{I_1 n}$	–	0.2	0.2	0.2	0.3
$w_3, w_{I_2 s}$	1.3	1.3	1.3	1.3	1.95
$w_{I_2 n}$	–	0.2	0.2	0.2	0.2
w_4	4	4	4	4	4
w_5	0	0.2	Varies	Varies	Varies
h_1	0.5	0.5	0.5	0.5	0.5
h_2	0.5	−3.7	−3.7	−3.7	−3.7
h_3	−0.5	−0.5	−0.5	−0.5	−0.5
l	0.1	0.1	0.1	0.1	0.1
τ_1	0.66	0.66	0.66	0.66	0.66
τ_2	100	100	100	100	40

2.4 Quantitative comparison between datasets

The EEG is thought to originate mainly from cortical sources, with various factors playing a role in the contribution such as source density, cortical folding and skull structure amongst others. The location of the sources, relative to the scalp electrode can also play a role. As a first approximation, we consider the mean of the excitatory variables in the DTI nodes which are closest in Euclidian space to the scalp electrode to be representative of the EEG output.

We compare differences between seizures within and between patients both simulated and also using clinical recordings. To this end, we use two measures of the spatiotemporal properties of the seizure, one linear (cross correlation, the MATLAB 'corr' function) and one nonlinear (mutual information as in Brown et al. (2011), bin size 100 using base 2 bit). Each measure is applied to each seizure and results in a 19 * 19 symmetric matrix which is a measure of correlation between 19 standard EEG channels. Aarabi et al. (2008) showed with a sliding window approach that both linear and nonlinear measures indicate stationarity during the course of absence seizures. We therefore applied these measures to the entire seizure using zero lag.

To calculate differences between seizures within and between patients the sum of the absolute value of differences between the matrices was taken. This single value indicates the variability in space and time between any two seizures. Larger values indicate greater variability (greater differences) between seizures.

Our clinical data includes 10 patients with clinically diagnosed absence epilepsy from The Department of Neurology, University Hospital Schleswig-Holsten in Kiel, Germany and

[2] http://surfer.nmr.mgh.harvard.edu.

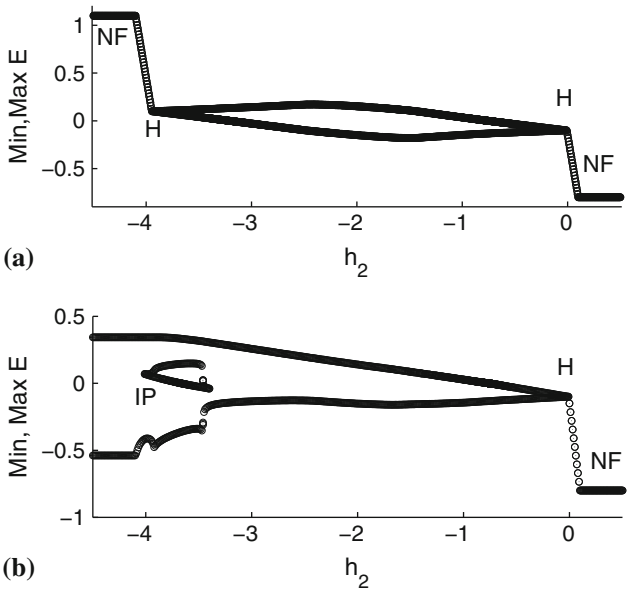

Fig. 2 Bifurcation diagram of the one compartment model (Eq. 1) using the PWL function as in Taylor and Baier (2011) scanning parameter h_2. **a** $w_5 = 0$; oscillations are bounded by Hopf bifurcations (H) at -4 and 0. The stable focus value next to the oscillatory region linearly increases (decreases) before becoming a stable node on the left (right) side at point NF. **b** $w_5 = 2$. Transition from a node to a focus (NF) at $h_2 = 0.25$ followed by a supercritical Hopf bifurcation (H) at $h_2 = 0$. Spike-wave oscillations occur between $h_2 \approx -3.6$ and $h_2 \approx -4$ where there is an inflection point (IP) as described by Rodrigues et al. (2010)

from The Department of Neurology, Inselspital, Bern, Switzerland (mean 4.2 seizures per patient, range 3–7 seizures per patient) sampled at 256 Hz and referenced using the Hjorth method. Further details of this patient data is included in the Supplementary online material (Supplementary Table 1). Our simulated data includes the use of DTI connectivity obtained from 10 healthy humans with 5 simulated seizures per person.

3 Results

3.1 Space-independent model

We begin our investigation by considering the simplest of our models, namely the one compartment case, Eq. 1, which represents local dynamics. To characterise its dynamics, we show two bifurcation diagrams of Eq. 1 as a function of the offset parameter h_2 in Fig. 2. In Fig. 2a, $w_5 = 0$, which reduces the system to two dimensions (the E/I_1 subsystem) with no influence from the slow inhibitory population. In Fig. 2b, we set $w_5 = 2$, which recovers the contribution of the slowly activating inhibitory population to the excitatory population E. The values of the other parameters were chosen following previous studies and include the possibility of spike-wave dynamics.

In Fig. 2a, for positive values of $h_2 > l$ (right side of the figure) the system is encountered in a stable node. Decreasing h_2 first leaves the node unaffected (between 0.5 and l) and then leads to linearly increasing fixed point values of E. In this linearly changing region, the fixed point is a stable focus. At $h_2 = 0$, there is a supercritical Hopf bifurcation which leaves the focus unstable and creates a limit cycle. This limit cycle begins with fixed frequency and zero amplitude at the bifurcation point and its amplitude subsequently increases as h_2 decreases until $h_2 \approx -1.5$. A further decrease of h_2 beyond $h_2 \approx -2.5$ leads to diminishing amplitudes until the limit cycle disappears in another supercritcal Hopf bifurcation at $h_2 = -4$ leading to a stable focus solution. The limit cycle frequency changes in the oscillatory region, increasing the closer it gets to the two bifurcation points. In the region $h_2 \lesssim -4.1$, there is again a single stable node solution.

The system incorporating a third variable displays identical dynamics to the two-dimensional system for $-2 \lesssim h_2$ as can be seen by comparing the right side of Fig. 2a, b. However, the limit cycle born for decreasing h_2 sustains an increase in amplitude as h_2 decreases until $h_2 \approx -3.6$. On the left side of the diagram, for $-5 < h_2 \lesssim -4.1$, there is a high-amplitude oscillation with a frequency that is considerably slower compared to the small-amplitude limit cycle described above. Bounded by these two simple periodic oscillations there is a limit cycle with two maxima and two minima in the region $-4 < h_2 < -3.6$. In this region, the waveform closely resembles the SWDs of absence seizures (Taylor and Baier 2011). Both the slow oscillations and the SWD are made possible by the addition of the third layer with the slowly activated inhibitory population. The information above provides a starting point for the investigation of coupled systems with multiple compartments in order to study the spatio-temporal features of the local network model Eq. 4.

3.2 Multiple coupled compartments: local connectivity

In principle, one could use a single compartment Eq. 1 as a 'node' to build up a large-scale model. Transitions from background to epileptic dynamics would then typically be modelled by parameter changes from a limit cycle behaviour with small amplitude and faster frequency to the SWD with slower frequency and comparatively large amplitude (as in Fig. 2b when parameter h_2 switches from, e.g. -3 to -3.5) or directly from a fixed point to SWD [parameter set as, e.g. in Taylor and Baier (2011)]. However, employing a more detailed neural mass model it was argued recently that nearest-neighbour local connectivity could induce plausible out-of-phase oscillatory behaviour deterministically to create an irregular rhythmic background activity in the spatial average (Goodfellow et al. 2010). To model the local transition to epileptic dynamics, we therefore approximate background

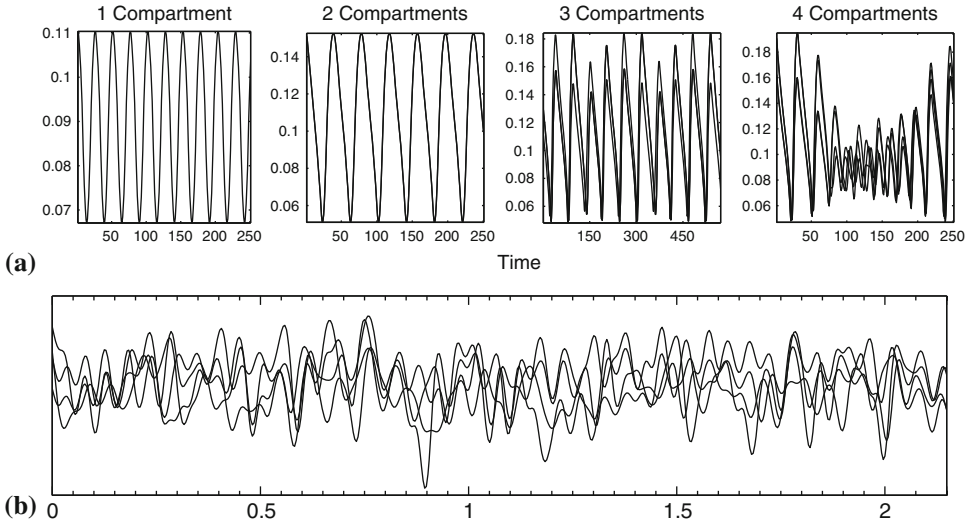

Fig. 3 Background dynamics of the spatially extended coupled system Eq. 4. **a** Time series of the excitatory variables of all compartments. *From left to right* Simple periodic oscillations in a single compartment; simple periodic, synchronised oscillations in two coupled compartments; complex periodic oscillations in three coupled compartments where only two variables have identical waveforms; temporally irregular and spatially desynchronised activity in four coupled compartments. **b** Clinical ECoG recordings from four neighbouring electrodes during an inter-ictal state without epileptiform features

activity in the same spirit by a small set of coupled compartments.

We consider the third layer (I_2) as being a requirement for the SWD activity to be present as this enables the appropriate minimal 'bursting' mechanism to robustly generate spike-wave model discharges (Taylor and Baier 2011). In order to investigate desynchronised background, one approach to take is to study the model without the third layer, whilst keeping all parameters constant in spatially coupled systems. In addition, if we seek to find a minimal model capable of producing the desired properties, we can take the approach of sequentially increasing the number of compartments. Figure 3 shows time series from systems of one, two, three and four coupled compartments where $h_2 = -3.7$ and $w_5 = h_3 = 0$ reverting the system to a two layer model (c.f. Fig. 2a).

Increasingly complex behaviour occurs up to four compartments. For only one compartment simple, regular oscillations occur. This is shown in Fig. 3a (left panel) and is essentially a time series from the bifurcation diagram in Fig. 2a. Using two coupled compartments (Fig. 3a, second panel), the model again produces simple regular oscillations although with a slower frequency. The two oscillators are phase synchronised and have identical waveforms in both compartments. In three coupled compartments (Fig. 3a, third panel), we still observe phase synchrony; however, two of the compartments have the same waveform and one does not. This causes a more complex repeating waveform. Finally, in four compartments (Fig. 3a, right panel), we obtain irregular, non-identical oscillatory waveforms which are present in all four compartments. In addition, changes in phase synchrony occur over time in the four compartment model (near the centre of the panel). Desynchrony and irregular, seemingly random waveforms are features present in inter-ictal EEG and ECoG. Figure 3b shows an electrocorticogram (ECoG) recording of neighbouring contacts. A single scalp EEG electrode is assumed to record the meanfield of an area the includes a number of ECoG contacts. Note the partial phase synchrony and irregular waveform in each contact and a tendency to wax and wane (compare the right panel of Fig. 3a). It is important to note that no noise or random term is added to the model in these simulations. The deterministic model produces the important feature of temporally irregular waveforms combined with spatial desynchrony. However, in contrast to previous modelling approaches which ignore the spatial component and add a random noise term, this now arises from the interactions between the four compartments.

We now include the third layer by using non-zero values for w_5 and h_3, the results of which are shown in Fig. 4. Figure 4 shows a diagram of regions of model output and exemplary time series of the different types of activity produced by the four compartment model. This is done using different parameter values of excitatory–excitatory coupling strength (w_{En}) and excitatory–slow inhibitory coupling strength (w_5). We numerically determine stable solutions, thus elucidating which dynamic regimes can be observed and where transitions between them take place, which suffices for the purposes of the current study. A systematic bifurcation analysis is left for future work.

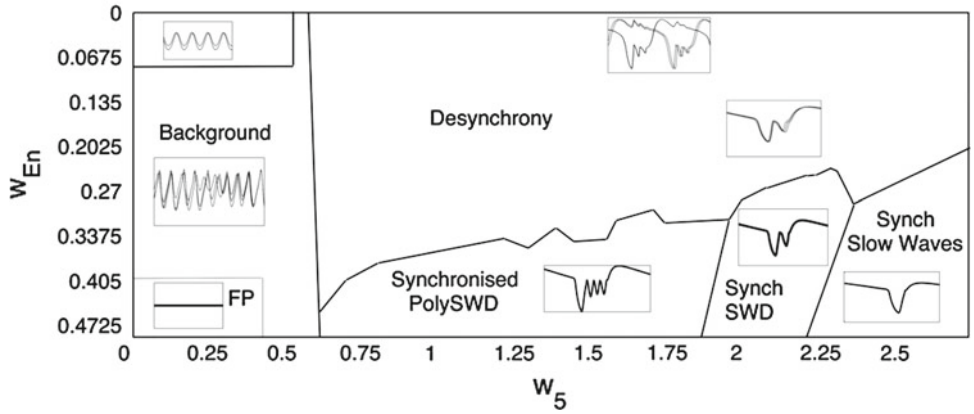

Fig. 4 Results from the four coupled compartment system. Diagram scanning w_{En} and w_5. Various regions of activity can be observed with exemplary time series of the excitatory variables shown in each inset. Each inset for $w_5 > 0.5$ shows one full cycle and is, therefore, representative of full model dynamics at the corresponding parameter values. $-E$ are plotted in the insets as in subsequent figures to aid in comparison. The diagram shows areas of synchronised activity which gets less synchronous for smaller values of w_{En} when w_5 is sufficiently large. For smaller values of w_5, low-amplitude oscillations and fixed point (FP) solutions are shown

For values of $w_5 < 0.5$, the system reverts to the dynamics of the two layer model. This is because $h_3 = -0.5$ and when $w_5 < |h_3|$ the contribution of the third variable to the excitatory variable is zero. When in the background state, the activity depends on the excitatory coupling. For small values of w_{En}, the desynchronised background activity dominates (Fig. 4, middle inset, left side). If the excitatory coupling is stronger the model goes to a fixed point solution (Fig. 4, inset at lower left corner). Our model therefore allows us to describe background dynamics by either a self-oscillating or a steady state dynamics.

Increasing the strength of w_5 increases the amount of input to the slow inhibitor from the excitatory location. If the strength of this input is greater than the h_3 offset then the slow inhibitor begins to influence the dynamics of the system. With active participation of the third population layer (using $w_5 > |h_3|$) there are areas of poly-spike-wave dynamics (polySWD), simple SWD and slow waves. All are synchronised when w_{En} is sufficiently large. Areas of polySWD and SWD are present for many values of w_{En}, meaning that the model can describe transitions from either the fixed point or the oscillatory background state to SWD using a change of parameter. For mid values of w_{En} (e.g. 0.2025), when w_5 is sufficiently large (e.g. 2) the waveforms are not perfectly synchronised; however, this degree of desynchrony is subtle and is dependent on w_{En}. An example of such subtle phase shifting leading to desynchrony is shown in the corresponding inset of Fig. 4. For smaller values of w_{En}, the polySWD or SWD become strongly phase shifted.

Due to the relationship between w_5 and h_3, instead of w_5 one can also use the stimulus parameter h_3 to take the system from background activity to the synchronised SWD (results not shown).

The model is, therefore, capable of producing a desynchronised background state using either two or three layers. We have also demonstrated that the model is capable of producing highly synchronised spike-wave dynamics. Furthermore, we have shown that there are possibilities for the model dynamics to change states by altering either the connectivity parameter w_5 or the stimulus parameter h_3. Figure 5 shows the time series of all four excit-

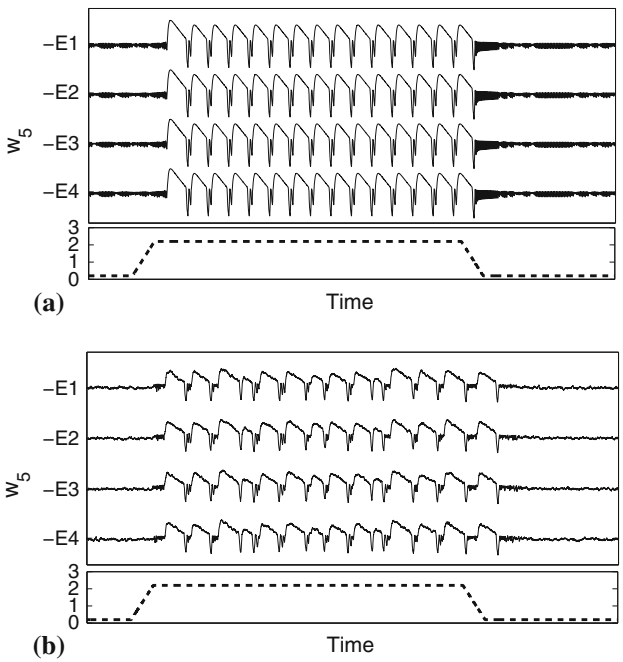

Fig. 5 Dynamics of spatially extended four compartment three layer model. **a** Transition from low-amplitude desynchronised oscillations to highly synchronised high-amplitude SWD caused by a gradual ramping in the connectivity parameter w_5 and back again where $w_{En} = 0.3$. **b** as in **a** except $w_{En} = 0.45$ and with additive noise in all variables

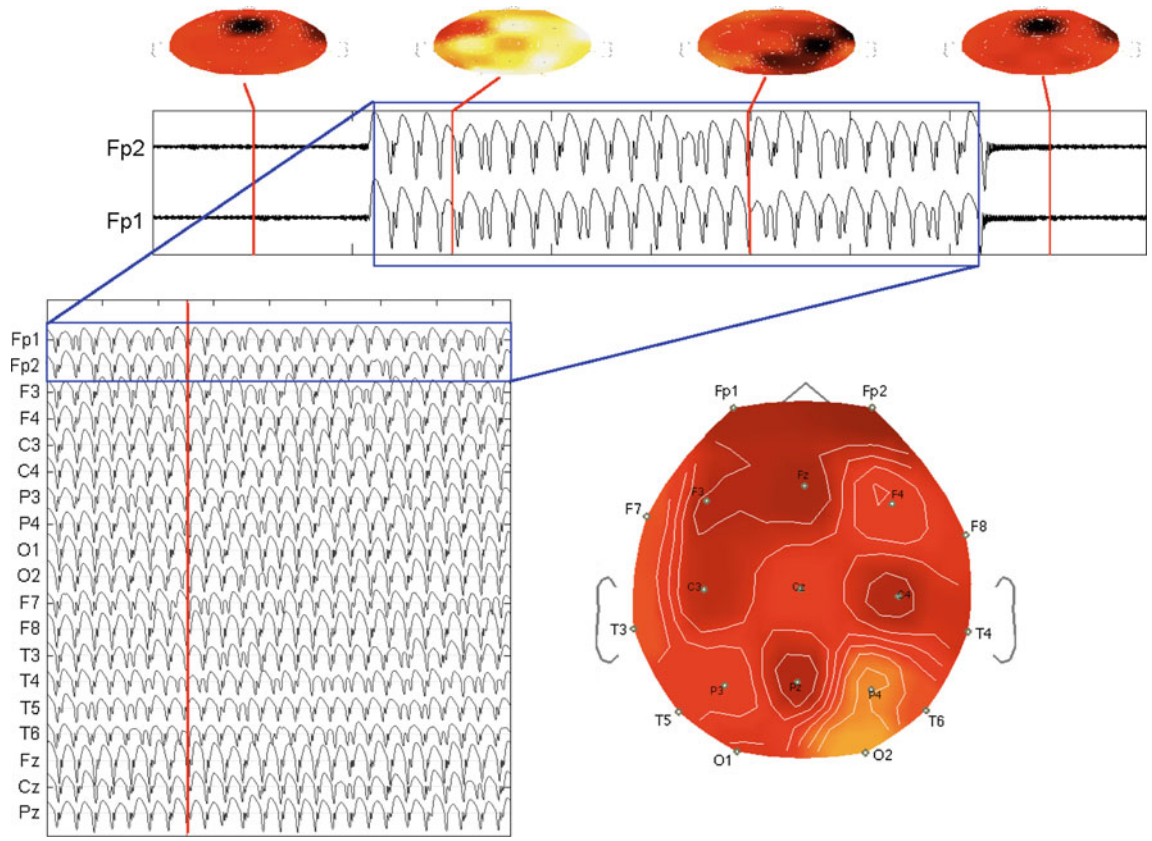

Fig. 6 Simulation results in the large-scale model (Eq. 5) with connectivity set 1, seizure 1. *Upper panels* Spatio-temporal activity at different time points shown as topological profiles. Zoom of two simulated channels (Fp2, Fp1). *Lower left panel* Time series of all 19 simulated channels. *Lower right panel* Interpolated topological profile at $t \approx 2.5$ s. Colour indicates variable value. Image is a modified still from Supplementary Movie 1 (Colour online)

atory variables using the four compartment model subject to a ramp in parameter w_5 which accounts for enhanced input to the slow inhibitory population. In Fig. 5a, $w_{En} = 0.3$ ensuring the background state has deterministic irregular desynchronised oscillations. In Fig. 5b, an alternative scenario is shown where $w_5 = 0.45$ and a noise term is added to all variables to model the background activity. We can therefore account for both approaches to the modelling of background activity in our model, i.e. deterministic irregular oscillations, or a fixed point plus noise. The first in agreement with Goodfellow et al. (2010), the second following the approach of Breakspear et al. (2006).

When changing the w_5 parameter in both cases from a value in the area of background state in the bifurcation diagram to a value in the SWD state and back again, we observe the apparently immediate onset and offset of SWD that is similar to observations in clinical EEG recordings. The sudden onset happens despite the fact that the parameter is ramped continuously and it occurs only after the parameter has reached its final value. If the mean of all excitatory variables is considered (as will be used in the next section) the transition occurs from highly irregular desynchronised background to strongly synchronised SWD in both cases.

The reported results qualitatively also hold true for larger systems with more complicated Gaussian distributed connectivity values (see Supplementary Fig. 1 for an example). Thus, we consider the four compartment model to be a robust prototype to describe the transition from irregular background to synchronous SWD.

3.3 Large-scale extension: long-range connectivity

Seizures were simulated in the large-scale model by ramping the w_5 parameter globally from the background state to the seizure state and back again. Random initial conditions were used for each simulation and the model was simulated in the background state until any transient activity had disappeared prior to any parameter ramping. The initial conditions at the point of seizure onset, whilst always in the background state, were, therefore, different.

In Fig. 6, we show an exemplary time series of the 19 simulated EEG channels along with a topological profile of activity in all spatial locations at $t \approx 2.5$ s into the seizure.

SWD, polySWD and slow wave oscillations can be observed in all simulated channels. There is some degree of irregularity in the oscillations in both space and time with regard to waveform and amplitude. For example, the amplitude of the oscillations in channel Fz are of higher amplitude than those in channel T6. In the topological heatmap (right panel, Fig. 6), a complex spatial activity profile can be observed. This spatial heatmap varies over time, a movie of which can be seen in Supplementary Online Movie 1 (SOM1). During SOM1 one can observe rapidly changing non-trivial spatio-temporal activity. It is important to emphasise that the simulation is not intended to reproduce patient-specific spatio-temporal features, rather more generic features common to all absence seizures, i.e. SWD, polySWD, slow waves, high synchrony, large amplitude and complex, non-trivial spatial profiles.

3.4 Quantitative comparisons between datasets

An important feature of clinical epilepsy is that seizures of a particular patient tend to evolve in stereotypical ways, which is a phenomenon known as stereotypy (Schindler et al. 2011). The interesting question of whether the complex spatio-temporal patterns observed in our large-scale simulations can support this feature was, therefore, investigated as follows.

Cross correlation and mutual information were used to study the impact of different connectivity structures on widespread spike-wave activity. In the upper panel of Fig. 7, comparisons are made between clinical datasets within patients (red asterisks) and between patients (black circles) for each of the 10 patients. In all cases, the seizures within patients are more similar than when the seizures are compared to other patients. In analysis of simulated seizures, the same is also true and is shown in the lower panel of Fig. 7. Similar results were also obtained using mutual information (Supplementary Fig. 2).

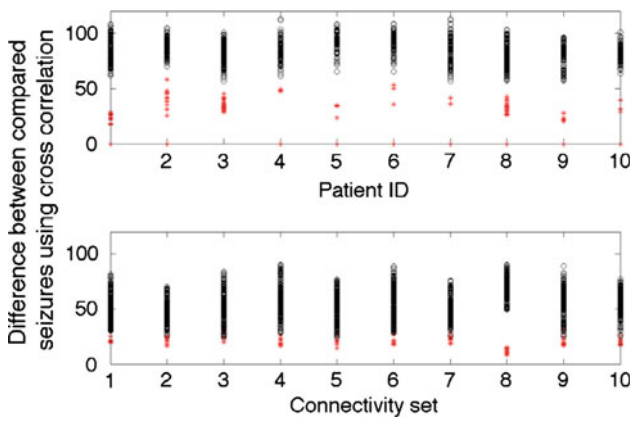

Fig. 7 Comparisons of seizures using cross correlation. Difference between two seizures from within the same patient (*red asterisks*) and the difference with a seizure from another patient (*black circles*). Larger values indicate the seizures are more different. *Upper panel* Results using clinical data. *Lower panel* Results using simulated seizures from different connectivity sets (Colour online)

4 Discussion

In this study, we presented a large-scale, patient-specific model for the investigation of spike-wave dynamics as seen during absence seizures in humans. In a discrete, hierarchical network approach, we demonstrated that a simplified local model of four coupled compartments was sufficient to capture key spatio-temporal dynamics relating to the transition between a desynchronised background state and the more highly correlated seizure state. Realistic long-range connectivity derived from human data was then incorporated into the model in order to extend to the larger spatial scale. We demonstrated that despite the inevitable heterogeneity of this anatomical network, transitions from background to SWD could still be modelled alongside non-trivial spatio-temporal dynamics. Beyond absence seizures, this approach can be applied to other forms of generalised epilepsies and also to partial epilepsies that present specific spatio-temporal seizure evolution patterns. Whereas previous approaches to model SWD often made the assumption of spatial homogeneity (Breakspear et al. 2006; Marten et al. 2009), modelling large-scale dynamics of abnormal rhythms with heterogeneities in the connectivity might be crucial for understanding patient-specific spatio-temporal features of, e.g. absence epilepsy (Garcia-Dominguez et al. 2005; Blumenfeld 2005; Moeller et al. 2008; Bai et al. 2010).

Our initial studies of the space-independent system demonstrated that the inclusion of a third variable in the Amari oscillator, namely, the slowly activating inhibitory population, led to qualitative changes in the system dynamics (Fig. 2). The three-dimensional system Eq. 1, therefore, supports a parameter-driven transition from background oscillations to spike-wave dynamics via the modulation of a model parameter. We demonstrated the specific case of this parameter being the strength of activation of an inhibitory population. This is in line with previous models of parameter driven transitions to SWD in space independent models (Marten et al. 2009; Breakspear et al. 2006) and adds evidence to the importance of connectivity between populations of excitatory and inhibitory neurons for transitions to seizure dynamics. In the current study, we have shown that this feature is preserved in higher dimensional representations of large-scale brain dynamics incorporating realistic long-range connectivity.

In extending the model spatially, several different prototypes for the number of compartments that could serve as representing local dynamics were considered. Borisyuk et al. (1995) used two coupled neural field oscillators in a similar approach, and observed complex periodic and chaotic

dynamics resulting from the coupling. We ultimately used four coupled compartments showing complex, partly desynchronised oscillations which in addition showed waxing and waning of the amplitudes consistent with ECoG recordings. This was chosen as a basis for further work and as a prototype for further spatial expansion. Four compartments is fitting with the original Amari model in that it is the smallest possible configuration which allows both symmetrically coupled and uncoupled neighbour(s) and is translationally invariant with periodic boundaries. This approach is compatible with previous studies of small networks of neural mass models to account for the dynamics of background rhythms (David and Friston 2003; David et al. 2005; Ursino et al. 2010). An alternative representation of the fluctuating EEG background state can be given by a model with noise driven steady states (e.g. Suffczynski et al. 2004; Breakspear et al. 2006 in models of transitions to the absence-like seizures). A limitation of this approach is that the nature of correlations between noisy inputs to different compartments is unknown. The approach of coupled asynchronous oscillators has been previously used by Goodfellow et al. (2010) and can produce irregular time series on the mean field, as confirmed in this study. However, the bifurcation scan Fig. 4 and time series Fig. 5 show that our model is able to implement both mechanisms depending on the exact choice of parameters.

We have shown that inter-ictal and ictal transitions can occur in our model. Specifically, this is achieved by gradually ramping the w_5 parameter between states. This parameter represents the connectivity from the excitatory populations to the slow inhibitory populations. Such a parameter has been hypothesised to represent dynamic inhibitory mechanisms operating on a slow time scale such as extracellular potassium, glial processes or subcortical (e.g. thalamic) input (Wang et al. 2012). This increased activation of such processes has been modelled in part in more detailed alternative model formulations. For example, Breakspear et al. (2006) showed that SWD can arise as a result of an increase in the parameter representative of connectivity strength from the cortex to a subcortical thalamic population. Furthermore, changes in levels of carbon dioxide, oxygen and pH due to hyperventilation have been biophysically implicated in such thalamocortical interactions (Sherwin 1967) and the absence seizures (Hughes 2009). The gradual decrease in our parameter w_5 can be compared to a return to the normal resting level of a property such as pH as a result of normal breathing.

We have used the Amari oscillator as a basis for our work; however, it is important to note that alternative models could be used instead. For example, recent studies using purely phenomenological models showed functional network structure (Benjamin et al. 2012) and excitability (Goodfellow et al. 2012b) can play a role in seizures. This approach of using simplified, less biophysically motivated models, has been used by other authors in similar studies of large-scale brain models (Honey and Sporns 2008; Deco et al. 2009). Alternatively, in future studies, the present simplified model for SWD can be substituted by models incorporating more physiological details (Breakspear et al. 2006; Marten et al. 2009; Goodfellow et al. 2010).

Modelling the spatio-temporal aspects of epileptiform EEG is a crucial step towards understanding the macroscopic mechanisms of epilepsy. In particular, even so-called generalised seizures are not spatially homogeneous events that can be sufficiently characterised by the production of SWD rhythms alone. References (Moeller et al. 2008) and (Bai et al. 2010), for example, revealed distinct spatial characteristics of SWD in humans. Furthermore, Holmes (2004) and Rodin and Ancheta (1987) have reported non-trivial spatial distributions of EEG rhythms during generalised seizures.

Combined EEG and fMRI of the absence seizures has shown patient-specific fingerprints (Moeller et al. 2010). The observed property of patient-specific features has been demonstrated in our model containing heterogeneous connectivity. Such a patient-specific property could not be shown in a homogeneous model of the cortex (Robinson et al. 2002). We have therefore demonstrated that the patient-specific connectivity is one potential explanation for the observed features.

In future studies, our model can be used for more detailed investigations of spatio-temporal dynamics and the underlying connectivity patterns using various other network topologies. This could include those from clinically diagnosed epileptic patients. This may be important as some authors have reported differences in large-scale epileptic networks in mesial temporal lobe epilepsy (Focke et al. 2008) and juvenile myoclonic epilepsy (Muircheartaigh et al. 2011). This preliminary study based on the extended Amari oscillator could be used in future to quantitatively compare clinical and simulated data similarly to other approaches (David et al. 2004). Until recently, most multivariate data analysis of epileptic EEG is done without reference to a specific spatio-temporal model of the phenomenon under observation whereas our model allows us to compare to multivariate properties at the level of the clinical EEG.

Such a model can also be used for the investigation of the proposed focal cortical onset of generalised seizures (Meeren et al. 2002), spatially localised 'focal' (simple partial) seizures, or secondary generalised seizures with a focal onset through the use of heterogeneous parameter ramping. Indeed, this technique could also be used to ramp only specific nodes in, for example the mesial frontal and orbito-frontal regions to study the patterns of propagation as suggested in Holmes (2004).

In this study, we formulated the large-scale framework to study patient-specific features of generalised SWD, comparing model output directly to clinical EEG. For general future purposes this might be supplemented with a more

realistic conversion of model variables to EEG signals in accordance with Westmijse et al. (2009), Bai et al. (2010). Various approaches of such forward models exist in the literature for population level mathematical models (Kiebel et al. 2006; Sotero et al. 2007; Valdes-Sosa et al. 2009; Cosandier-Rimele et al. 2010). In addition, comparisons to fMRI data can be made by including a model to account for the hemodynamic response (Friston et al. 2003; Valdes-Sosa et al. 2009). It will be of interest to infer features of functional connectivity and compare to underlying structural networks in the case of generalised seizures (Zhang et al. 2011).

Acknowledgments We thank H. Muhle, M. Siniatchkin, F. Möller and U. Stephani, Neurology, University Hospital Kiel and K. Schindler, Department of Neurology, Inselespital, Bern, CH for clinical EEG data and discussion of neurological matters. We acknowledge financial support form EPSRC and BBSRC. PNT thanks G. Parker and M. Muldoon for discussion. We thank C. Rummel, M. Müller and G. Leaver for discussion.

References

Aarabi A, Wallois F, Grebe R (2008) Does spatiotemporal synchronization of EEG change prior to absence seizures?. Brain Res 1188:207–221

Amari S (1977) Dynamics of pattern formation in lateral-inhibition type neural fields. Biol Cybern 27(2):77–87

Amor F, Rudrauf D, Navarro V, Ndiaye K, Garnero L, Martinerie J, LeVanQuyen M (2005) Imaging brain synchrony at high spatiotemporal resolution: application to MEG signals during absence seizures. Signal Process 85(11):2101–2111

Babajani-Feremi A, Soltanian-Zadeh H (2010) Multi-area neural mass modeling of EEG and MEG signals. NeuroImage 52(3):793–811

Bai X, Vestal M, Berman R, Negishi M, Spann M, Vega C, Desalvo M, Novotny EJ, Constable RT, Blumenfeld H (2010) Dynamic time course of typical childhood absence seizures: EEG, behavior, and functional magnetic resonance imaging. J Neurosci 30(17):5884

Benjamin O, Fitzgerald THB, Ashwin P, Tsaneva-Atanasova K, howdhury F, Richardson MP, Terry JR (2012) A phenomenological model of seizure initiation suggests net-work structure may explain seizure frequency in idiopathic generalised epilepsy. J Math Neurosc 2(1):1

Blumenfeld H (2005) Cellular and network mechanisms of spike-wave seizures. Epilepsia 46:21–33

Bojak I, Oostendorp TF, Reid AT, Kotter R (2010) Connecting mean field models of neural activity to EEG fMRI data. Brain Topogr 23(2):139–149

Borisyuk GN, Borisyuk RM, Khibnik AI, Roose D (1995) Dynamics and bifurcations of two coupled neural oscillators with different connection types. Bull Math Biol 57(6):809–840

Breakspear M, Stam CJ (2005) Dynamics of a neural system with a multiscale architecture. Philos Trans R Soc B Biol Sci 360(1457):1051–1074

Breakspear M, Roberts JA, Terry JR, Rodrigues S, Mahant N, Robinson PA (2006) A unifying explanation of primary generalized seizures through nonlinear brain modeling and bifurcation analysis. Cereb Cortex 16(9):1296

Brown G, Pocock A, Zhao M, Lujan M (2011) Conditional likelihood maximisation: a unifying framework for mutual information feature selection. J Mach Learn Res 13:26–46

Cohn R, Leader HS (1967) Synchronization characteristics of paroxysmal EEG activity. Electroencephalogr Clin Neurophysiol 22(5):421–428

Cosandier-Rimele D, Merlet I, Bartolomei F, Badier JM, Wendling F (2010) Computational modeling of epileptic activity: from cortical sources to EEG signals. J Clin Neurophysiol 27(6):465

David O, Friston KJ (2003) A neural mass model for MEG EEG: coupling and neuronal dynamics. NeuroImage 20(3):1743–1755

David O, Cosmelli D, Friston KJ (2004) Evaluation of different measures of functional connectivity using a neural mass model. NeuroImage 21(2):659–673

David O, Harrison L, Friston KJ (2005) Modelling event-related responses in the brain. NeuroImage 25(3):756–770

Deco G, Jirsa V, McIntosh AR, Sporns O, Kotter R (2009) Key role of coupling, delay, and noise in resting brain fluctuations. Proc Natl Acad Sci USA 106(25):10302

Deco G, Jirsa VK, McIntosh AR (2011) Emerging concepts for the dynamical organization of resting-state activity in the brain. Nat Rev Neurosci 12(1):43–56

Eeckman FH, Freeman WJ (1991) Asymmetric sigmoid non-linearity in the rat olfactory system. Brain Res 557(1–2):13–21

Focke NK, Yogarajah M, Bonelli SB, Bartlett PA, Symms MR, Duncan JS (2008) Voxel-based diffusion tensor imaging in patients with mesial temporal lobe epilepsy and hippocampal sclerosis. NeuroImage 40(2):728–737

Friston KJ, Harrison L, Penny W (2003) Dynamic causal modelling. NeuroImage 19(4):1273–1302

Garcia-Dominguez L, Wennberg RA, Gaetz W, Cheyne D, Snead OC, Velazquez JLP (2005) Enhanced synchrony in epileptiform activity? Local versus distant phase synchronization in generalized seizures. J Neurosci 25(35):8077

Goodfellow M, Schindler K, Baier G (2011) Intermittent spike-wave dynamics in a heterogeneous, spatially extended neural mass model. NeuroImage 55(3):920–932

Goodfellow M, Schindler K, Baier G (2012a) Self-organised transients in a neural mass model of epileptogenic tissue dynamics. NeuroImage 59(3):2644–2660

Goodfellow M, Taylor PN, Wang Y, Garry DJ, Baier G (2012b) Modelling the role of tissue heterogeneity in epileptic rhythms. Eur J Neurosci 36(2):2178–2187

Holmes MD, Brown M, Tucker DM (2004) Are generalized seizures truly generalized evidence of localized mesial frontal and frontopolar discharges in absence. Epilepsia 45(12):1568–1579

Honey CJ, Sporns O (2008) Dynamical consequences of lesions in cortical networks. Hum Brain Mapp 29(7):802–809

Hughes JR (2009) Absence seizures: a review of recent reports with new concepts. Epilepsy Behav 15(4):404–412

Jansen BH, Rit VG (1995) Electroencephalogram and visual evoked potential generation in a mathematical model of coupled cortical columns. Biol Cybern 73(4):357–366

Jirsa VK, Kelso JAS (2000) Spatiotemporal pattern formation in neural systems with heterogeneous connection topologies. Phys Rev E 62(6):8462–8465

Jirsa VK, Sporns O, Breakspear M, Deco G, McIntosh AR (2010) Towards the virtual brain: network modeling of the intact and the damaged brain. Arch Ital Biol 148(3):189–205

Kiebel SJ, David O, Friston KJ (2006) Dynamic causal modelling of evoked responses in EEG MEG with lead field parameterization. NeuroImage 30(4):1273–1284

Marten F, Rodrigues S, Benjamin O, Richardson MP, Terry JR (2009) Onset of polyspike complexes in a mean-field model of human electroencephalography and its application to absence epilepsy. Philos Trans R Soc A Math Phys Eng Sci 367(1891):1145

Meeren HKM, Pijn JPM, Van Luijtelaar ELJM, Coenen AML, Lopesda Silva FH (2002) Cortical focus drives widespread corticothalamic

networks during spontaneous absence seizures in rats. J Neurosc 22(4):1480

Moeller F, Siebner HR, Wolff S, Muhle H, Granert O, Jansen O, Stephani U, Siniatchkin M (2008) Simultaneous EEG-fMRI in drug-naive children with newly diagnosed absence epilepsy. Epilepsia 49(9):1510–1519

Moeller F, LeVan P, Muhle H, Stephani U, Dubeau F, Siniatchkin M, Gotman J (2010) Absence seizures: individual patterns revealed by EEG-fMRI. Epilepsia 51(10):2000–2010

Muircheartaigh JO, Vollmar C, Barker GJ, Kumari V, Symms MR, Thompson P, Duncan JS, Koepp MJ, Richardson MP (2011) Focal structural changes and cognitive dysfunction in juvenile myoclonic epilepsy. Neurology 76(1):34–40

Parker GJM, Stephan KE, Barker GJ, Rowe JB, MacManus DG, Wheeler-Kingshott CAM, Ciccarelli O, Passingham RE, Spinks RL, Lemon RN et al. (2002a) Initial demonstration of in vivo tracing of axonal projections in the macaque brain and comparison with the human brain using diffusion tensor imaging and fast marching tractography. NeuroImage 15(4):797–798

Parker GJM, Wheeler-Kingshott CAM, Barker GJ (2002b) Estimating distributed anatomical connectivity using fast marching methods and diffusion tensor imaging. IEEE Trans Med Imaging 21(5):505–512

Parker GJM, Haroon HA, Wheeler-Kingshott CAM (2003) A framework for a streamline-based probabilistic index of connectivity (pico) using a structural interpretation of mri diffusion measurements. J Magn Reson Imaging 18(2):242–254

Pinault D, O'Brien TJ (2005) Cellular and network mechanisms of genetically-determined absence seizures. Thalamus Relat Syst 3(3):181

Robinson PA, Rennie CJ, Rowe DL (2002) Dynamics of large-scale brain activity in normal arousal states and epileptic seizures. Phys Rev E 65(4):041924

Rodin E, Ancheta O (1987) Cerebral electrical fields during petit mal absences. Electroencephalogr Clin Neurophysiol 66(6):457–466

Rodrigues S, Barton D, Marten F, Kibuuka M, Alarcon G, Richardson MP, Terry JR (2010) A method for detecting false bifurcations in dynamical systems: application to neural-field models. Biol Cybern 102(2):145–154

Rose CJ, Morris D, Haroon H, Embleton K, Logothetis N, RalphLambon M, Parker GJ (2009) Piconmat.com version 2.0: a web-based probabilistic tractography data service

Schindler K, Gast H, Stieglitz L, Stibal A, Hauf M, Wiest R, Mariani L, Rummel C (2011) Forbidden ordinal patterns of periictal intracranial EEG indicate deterministic dynamics in human epileptic seizures. Epilepsia 52:1771–1780

Sherwin I (1967) Alterations in the non-specific cortical afference during hyperventilation. Electroencephalogr Clin Neurophysiol 23:532–538

Sotero RC, Trujillo-Barreto NJ, Iturria-Medina Y, Carbonell F, Jimenez JC (2007) Realistically coupled neural mass models can generate EEG rhythms. Neural Comput 19(2):478–512

Suffczynski P, Kalitzin S, Lopes Da Silva FH (2004) Dynamics of non-convulsive epileptic phenomena modeled by a bistable neuronal network. Neuroscience 126(2):467–484

Taylor PN, Baier G (2011) A spatially extended model for macroscopic spike-wave discharges. J Comput Neurosci 31(3):679–684

Ursino M, Cona F, Zavaglia M (2010) The generation of rhythms within a cortical region: analysis of a neural mass model. NeuroImage 52(3):1080–1094

Valdes-Sosa PA, Sanchez-Bornot JM, Sotero RC, Iturria-Medina Y, Aleman-Gomez Y, Bosch-Bayard J, Carbonell F, Ozaki T (2009) Model driven EEG fMRI fusion of brain oscillations. Hum Brain Mapp 30(9):2701–2721

Wang Y, Goodfellow M, Taylor PN, Baier G (2012) A phase space approach for modelling of epileptic dynamics. Phys Rev E 85:061918

Weir B (1965) The morphology of the spike-wave complex. Electroencephalogr Clin Neurophysiol 19(3):284–290

Wendling F, Bartolomei F, Bellanger JJ, Chauvel P (2002) Epileptic fast activity can be explained by a model of impaired GABA ergic dendritic inhibition. Eur J Neurosci 15(9):1499–1508

Westmijse I, Ossenblok P, Gunning B, VanLuijtelaar G (2009) Onset and propagation of spike and slow wave discharges in human absence epilepsy: a MEG study. Epilepsia 50(12):2538–2548

Wilson HR, Cowan JD (1972) Excitatory and inhibitory interactions in localized populations of model neurons. Biophys J 12(1):1–24

Zhang Z, Liao W, Chen H, Mantini D, Ding JR, Xu Q, Wang Z, Yuan C, Chen G, Jiao Q (2011) Altered functional–structural coupling of large-scale brain networks in idiopathic generalized epilepsy. Brain 134(10):2912–2928